ACS APPLIED MATERIALS & INTERFACES

www.acsami.org

Research Article

Efficient Reduction of Selenite to Elemental Selenium by Liquid-Phase Catalytic Hydrogenation Using a Highly Stable Multiwalled Carbon Nanotube-Supported Pt Catalyst Coated by N-Doped Carbon

Yuhan Sun, Minghui Li, Xiaolei Qu, Shourong Zheng, Pedro J. J. Alvarez, and Heyun Fu*

Cite This: *ACS Appl. Mater. Interfaces* 2021, 13, 29541−29550

Read Online

ACCESS | Metrics & More | Article Recommendations | Supporting Information

ABSTRACT: A stable catalyst, Pt/carbon nanotube (CNT) coated with N-doped carbon (Pt/CNT@CN), was designed to reduce selenite (Se(IV)) in water to elemental selenium by liquid-phase catalytic hydrogenation. Commercial Pt/C, pristine Pt/CNT, and carbon-coated Pt/CNT (Pt/CNT@C) were used for benchmarking. The Pt particles in Pt/CNT@CN were completely embedded beneath the coatings to minimize leaching and were not easily accessible to Se(IV). However, Schottky−Mott-type metal−carbon junctions that activate H_2 were formed on the coated catalyst, facilitating effective reduction of Se(IV). The initial activity of Pt/CNT@CN (900.5 mg L^{-1} g_{cat}^{-1} h^{-1}) was two times higher than that of commercial Pt/C (448.6 mg L^{-1} g_{cat}^{-1} h^{-1}). The commercial Pt/C and uncoated Pt/CNT lost their initial activities during reuse and were almost inactive after 10 cycles due to significant Pt leaching (>90%) during the reaction and acid-washing regeneration processes. Pt/CNT@CN maintained 33% of the initial activity after the first cycle and stabilized over the following 9 cycles due to effective protection of Pt particles by carbon coatings. After 10 cycles, the activity of Pt/CNT@CN was over 20 times higher than that of Pt/C and uncoated Pt/CNT. Overall, catalytic hydrogenation using carbon-coated-supported Pt catalysts is an effective and promising approach to remove Se(IV) in water.

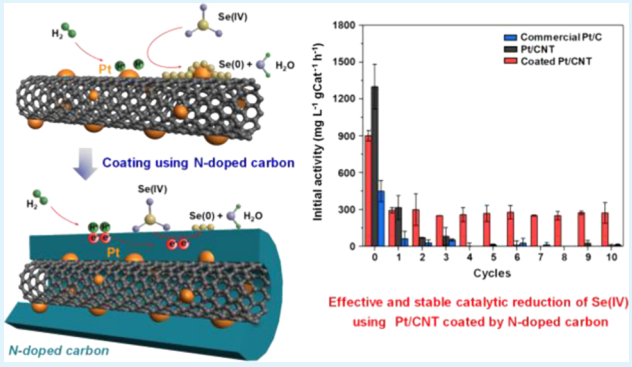

KEYWORDS: *carbonization, metal-support interaction, heterojunction, consecutive reduction kinetics, liquid-phase reduction*

INTRODUCTION

Selenium (Se) is a commonly found contaminant in water from both natural sources and anthropogenic activities such as agricultural irrigation, industrial production, mining, and coal combustion.[1−3] Se is an essential trace element for human health but can also be toxic at high concentrations (>400 μg day^{-1}).[4−6] The World Health Organization (WHO) has set the maximum guideline concentration for Se as 40 μg L^{-1} in drinking water.[7] The United States Environmental Protection Agency (U.S. EPA) limits Se concentration in drinking water to less than 50 μg L^{-1},[8] and sets the aquatic life ambient water quality criterion for Se to be 3.1 μg L^{-1}.[9] In natural systems, Se can cause fish kills and deformities of aquatic birds.[10,11] Se occurs in several valence states including selenate (Se(VI)), selenite (Se(IV)), elemental Se (Se(0)), selenide (Se(-II)), and organic Se. Se(VI) and Se(IV) are of greatest concern due to their high mobility and toxicity.[12−16] The acute toxicity of Se(IV) was reported to be almost 10 times higher than that of Se(VI).[15,16] Therefore, the removal of Se species from water, particularly Se(IV), is important.

Adsorption technologies have been widely used to remove Se(IV) from water, but safe disposal of the spent adsorbent is challenging. Reductive treatment of Se(IV) is an attractive alternative. Various reduction techniques have been explored to tackle Se(IV) pollution, including anaerobic bacteria, semiconductor photocatalysts, and zero-valent iron.[16−23] Nevertheless, these processes also require further treatment and disposal of by-products.[24−26] The liquid-phase catalytic hydrogenation reduction using H_2 as a reductant is an emerging and relatively green alternative for the removal of oxidized priority pollutants in water.[27−30] However, catalytic hydrogenation reduction of Se(IV) relies on noble metals (*e.g.*, Pt, Pd, Ru) that would be occluded and deactivated by deposition of the reduction product, Se(0), which represents a

Received: March 18, 2021
Accepted: June 7, 2021
Published: June 16, 2021

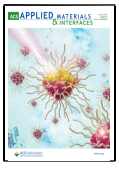

https://doi.org/10.1021/acsami.1c05101
ACS Appl. Mater. Interfaces 2021, 13, 29541−29550

major barrier. Additionally, the spent catalysts commonly undergo a harsh regeneration treatment (*e.g.*, high-temperature calcination and acid washing),[31−34] resulting in significant loss of the noble metal particles and associated deactivation.[31,32] This underscores the need for novel approaches to protect the noble metals from deactivation and leaching.

Carbon coating may effectively prevent noble metal loss during the reaction and regeneration process.[35,36] Carbon and metal can form a Schottky−Mott type junction that facilitates electron transfer from the Fermi energy level of the metal to that of carbon coating, which can then activate H_2.[31] As a result, carbon-coated metal catalysts display high activity and stability in several catalytic hydrogenation reactions.[37−39] We have recently shown that carbon-coated Pt efficiently catalyzes Cu(II) reduction, and the coating significantly mitigates Pt deactivation by Cu(0) deposition.[31] However, pristine carbon coatings are commonly negatively charged and have low adsorption affinity to anions like Se(IV) due to the electrostatic repulsion.[35] Thus, N-doping (which is commonly used to tune the surface chemistry of carbon materials[40,41]) might be a practical novel approach to introduce positively charged sites and increase surface hydrophilicity[42,43] to enhance Se(IV) adsorption and subsequent reduction.

In this study, we coated a multiwalled carbon nanotube (CNT)-supported Pt catalyst using conductive N-doped carbon (Pt/CNT@CN), and applied it for catalytic hydrogenation reduction of Se(IV) in aqueous solutions. CNT was selected as the support material because of its good chemical stability, high surface area that allows good Pt dispersion, and high conductivity that facilitates the electron transfer during Se(IV) reduction.[44] The CN coating was prepared by the direct carbonization of the precoated polyaniline (PANI) layer at different temperatures. Catalyst properties, including activity and stability for Se(IV) reduction, were characterized in detail to better understand the key factors controlling performance. The performance was benchmarked against commercial carbon-supported Pt catalyst (Pt/C), pristine Pt/CNT, and Pt coated by undoped carbon (Pt/CNT@C).

MATERIALS AND METHODS

Materials. Sodium selenite (Na_2SeO_3, >99%) was purchased from Nanjing Chemical Reagent Co., Ltd., China. Chloroplatinic(IV) acid ($H_2PtCl_6{\cdot}6H_2O$, >99.5%), ammonium persulfate (APS, >99.5%), and glucose were purchased from Shanghai Sinopharm Chemistry Co. Ltd., China. Aniline (>99.5%) was purchased from Sigma-Aldrich and was purified by distillation at reduced pressure prior to use. Acetic acid (HAc, >99.5%) and sodium acetate (NaAc, >99%) were also purchased from Sigma-Aldrich. The other reagents used in this study are of analytic grade and were purchased from Nanjing Chemical Reagent Co., Ltd. The multiwalled carbon nanotube (CNT) was obtained from Shenzhen Nanotech Port Co., Ltd., China. It was pretreated to remove amorphous carbon by calcination at 350 °C for 0.5 h, and the trace metals were removed by the acid oxidation method using 8 M HNO_3 at 90 °C for 8 h. Commercial Pt/C (Pt content of 5.0 wt %) was purchased from Aladdin Chemical Co., Ltd., China. Deionized water (18.2 MΩ·cm electrical resistance at 25 °C) was obtained from an ELGA Labwater system (PURELAB Ultra, ELGA LabWater Global Operations, U.K.) and was used in all of the experiments.

Preparation and Characterization of the Catalysts. CNT-supported Pt catalyst (Pt/CNT) was prepared by the conventional impregnation method.[45] The detailed preparation procedure can be found in the Supporting Information (SI). To prepare N-doped carbon (CN)-coated Pt/CNT (*i.e.*, Pt/CNT@CN), the Pt/CNT was first coated by a polyaniline (PANI) layer (*i.e.*, Pt/CNT@PANI) by the polymerization of aniline in the presence of APS.[46,47] Briefly, 7.5 mL of distilled aniline monomer was mixed with 1.0 g of Pt/CNT at 0 °C in an ice-water bath under stirring (pH 2.0), and aniline polymerization was initiated upon the addition of 1 mol L^{-1} APS (50 mL). The polymerization predominantly occurred on the surface of Pt/CNT because, under acidic conditions, the aniline monomer was adsorbed on the negatively charged surface of the CNT through the electrostatic attractive interaction.[46] After stirring for 8 h to reach complete polymerization, the Pt/CNT@PANI was recovered by filtration, rinsed with deionized water, and dried at 60 °C under vacuum for 12 h. Then, Pt/CNT@PANI was carbonized at a given temperature (*i.e.*, 500−800 °C) with a ramping rate of 5 °C min^{-1} for 5 h under a N_2 atmosphere. The resulting catalysts were denoted Pt/CNT@CN-*X*, where *X* is the carbonization temperature. For comparison, Pt/CNT coated by pure carbon layer (Pt/CNT@C-700) with a similar Pt content as that of Pt/CNT@CN-700 was prepared using the hydrothermal method (see details in the SI).[31] Prior to use, catalysts were grounded and sieved through a 400-mesh sieve (<37 μm) to exclude the potential internal mass transfer resistance.[48] The catalysts were characterized using a variety of techniques including inductively coupled plasma emission spectrometry (ICP-AES), X-ray photoelectron spectroscopy (XPS), transmission electron microscopy (TEM), energy-dispersive spectroscopy (EDS) mapping, X-ray diffraction (XRD), Raman spectroscopy, CO chemisorption, static contact angle, measurement of the points of zero charges (PZCs), and electrochemical impedance spectra (EIS) test. A detailed description of the characterization methods is given in the SI.

Batch Reaction Experiments. The performance of the catalysts for the liquid-phase reduction of Se(IV) was evaluated in a batch mode in a 250 mL four-flask reactor equipped with a pH meter. The reaction temperature was controlled at 25 °C in a thermostatic bath (SDC-6, Scientz Co., China). Briefly, 4 mL of Se(IV) stock solution (1000 mg L^{-1}) was mixed with 196 mL of a HAc-NaAc buffer solution (pH 4.75) under vigorous stirring (1500 rpm) to obtain a 200 mL of reaction solution with initial Se(IV) concentration of 20 mg L^{-1}. Then, 30 mg of the catalyst was dispersed in the solution, which was purged by N_2 with a rate of 200 mL min^{-1} controlled by a mass flowmeter (LZB-3WB, Horibametron Co., China) for 0.5 h to remove the dissolved oxygen. Under the above batch reaction conditions, less than 5% Se(IV) decreased due to adsorption on the catalyst surface (Figure S1 in the SI). The reduction reaction was initiated when the N_2 flow was switched to the H_2 flow (200 mL min^{-1}). Samples were collected at preset time intervals, filtered through a 0.45 μm filter membrane, and the concentrations of soluble Se(IV) were analyzed by ion chromatography (ICS1100, Dionex) using 20 mmol L^{-1} KOH as the mobile phase. The samples with low Se(IV) concentrations were analyzed by an inductively coupled plasma mass spectrometer (ICP-MS, NexIon300X, PerkinElmer). The limit of detection (LOD) of Se(IV) was found to be 0.15 mg L^{-1} by ion chromatography and 0.04 μg L^{-1} by ICP-MS.

A separate set of experiments were carried out to examine the effect of the solution pH on the catalyst activity. The pH was set from 3.0 to 9.0 using suitable buffers (10 mmol L^{-1}): HAc-NaAc for samples of pH 3.0−4.75, HAc-NH_4Ac for samples of pH 6.0, and Tris−HCl for samples of pH 7.5−9.0. The catalytic stability for Se(IV) reduction of the Pt-based catalysts was evaluated using consecutive catalytic reaction experiments. After each cycle of reaction, the used catalyst was collected by filtration and was regenerated by immersion in the mixture of concentrated HCl and HNO_3 (2:1, v/v) to remove surface deposited Se(0). The regenerated catalyst was subjected to sequential catalytic reaction and regeneration cycles. To test the practical application potential of Pt/CNT@CN, catalytic hydrogenation reduction of Se(IV) over Pt/CNT@CN-700 was conducted in different water matrices. Three water samples were collected from the Xuanwu Lake in the downtown of Nanjing City, a well in the residential area of the Nanjing City, and the tap water on the campus, respectively. The samples were filtered through 0.45 μm membranes and stored at 4 °C before use. Sample characteristics including salinity, electrical conductivity, total dissolved solids, total organic carbon (TOC), dissolved oxygen, and pH are summarized in Table

https://doi.org/10.1021/acsami.1c05101
ACS Appl. Mater. Interfaces 2021, 13, 29541−29550

Table 1. Structural Properties of Different Pt-Based Catalysts

catalysts	Pt loading amount (wt %)[a]	Pt particle size (nm)[b]	coating thickness (nm)[b]	CO sorption (μmol g^{-1})	PZCs[c]	contact angle (°)[d]
Pt/CNT	0.75	2.96	NA[e]	6.9	<2.0	106.8
Pt/CNT@C-700	0.38	4.52	6.39	BDL[f]	3.05	125.3
Pt/CNT@CN-700	0.35	4.71	7.71	BDL[f]	7.24	59.1
Pt/CNT after use	0.06	5.23	NA[e]	BDL[f]	<2.0	100.1
Pt/CNT@CN-700 after use	0.33	4.51	7.67	BDL[f]	5.21	59.5

[a]Determined by ICP-AES. [b]Calculated on the basis of TEM images. [c]Determined by acid−base titration. [d]Determined by static water contact angle measurements. [e]Not applicable. [f]Below the detection limit.

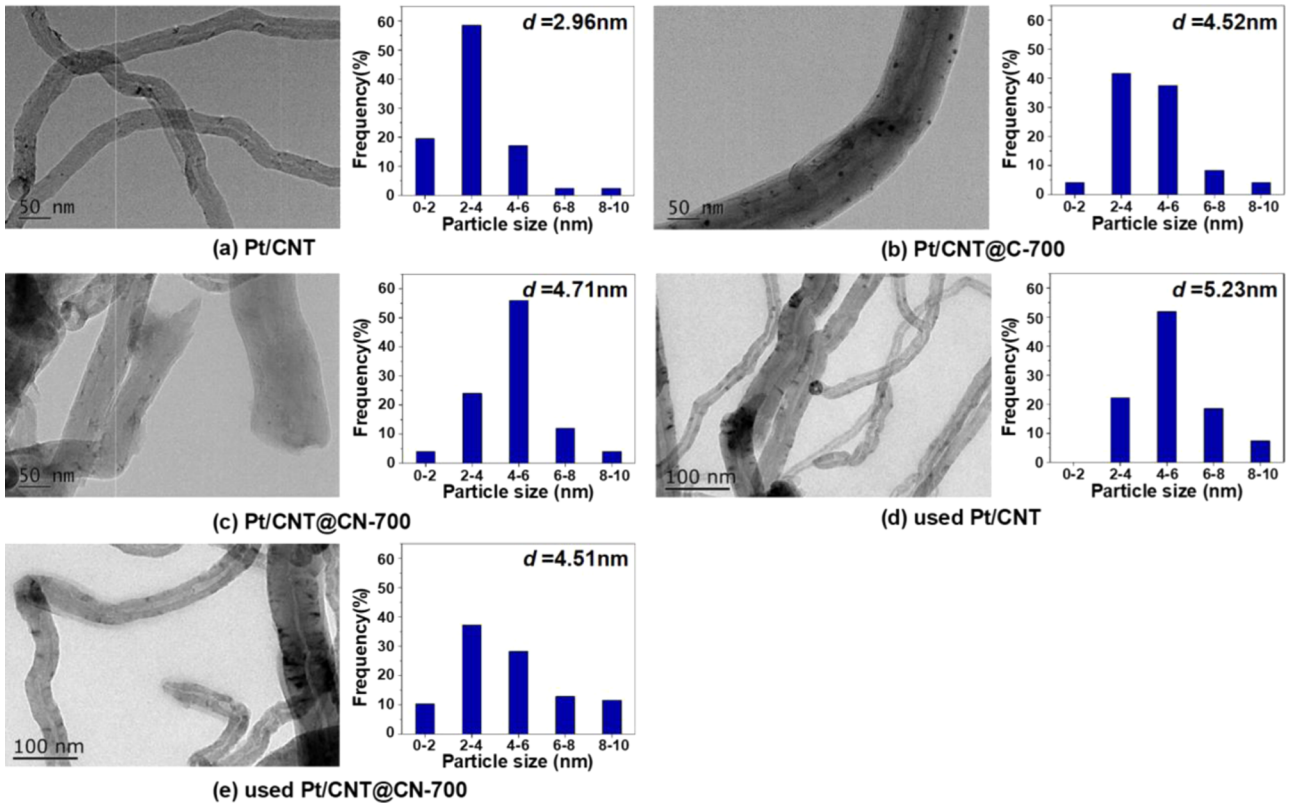

Figure 1. TEM images and particle size distributions of (a) Pt/CNT, (b) Pt/CNT@C-700, (c) Pt/CNT@CN-700, (d) Pt/CNT after use, and (e) Pt/CNT@CN-700 after use.

S1 in the SI. The Se(IV) concentrations in the water samples were measured to be 0.72, 0.84, and 0.57 μg L^{-1} for tap water, well water, and Xuanwu Lake water, respectively, all below the aquatic life criterion for Se. The water samples were spiked with 20 mg L^{-1} Se(IV) for reaction tests.

The initial activity r_0 (mg L^{-1} g_{cat}^{-1} h^{-1}) was defined as the reduced concentration of Se(IV) per gram of catalyst per hour in the initial 10 min. For all reactions, the initial Se(IV) conversion was below 25% to avoid inhibition by Se(0) deposition on the catalyst surface. To verify the absence of mass transfer limitations in the catalytic reaction, the catalytic reduction of Se(IV) on Pt/CNT@CN-700 was conducted in the presence of a series of catalyst dosages. As shown in Figure S2, the r_0 values normalized by the catalyst dosage were constant. Additionally, the Sherwood number and Thiele modulus were calculated to be far below 1.0 (results are presented in Table S2 in the SI). These results indicated the absence of mass transfer resistance under our experimental conditions.[48]

Statistical Analysis. All reaction data except the controls were collected in triplicate. The data were presented as mean value ± standard deviation. A two-tailed Student's *t*-test was used for statistical analysis. Statistical significance was indicated by $p < 0.05$.

RESULTS AND DISCUSSION

Structural Properties of Pristine and Coated Pt/CNT Catalysts. The Pt loading amounts for Pt/CNT, Pt/CNT@C-700, and Pt/CNT@CN-700 catalysts were 0.75, 0.38, and 0.35 wt % as measured by ICP-AES (Table 1), respectively. Pt/CNT@CN-700 had a surface N content of 6.71 at %, which mainly consisted of pyridinic N, pyrrolic N, and graphitic N (determined by XPS, Figure S3 and Table S3 in the SI). For Pt/CNT, diffraction peaks were observed at 2θ of 26.4, 42.2, and 44.4°, ascribed to the (002), (100), and (101) planes of the graphitic carbon in CNT (JCPDS No. 41-1487, Figure S4).[49] The characteristic diffraction peaks of metallic Pt were shown at 39.8° (111), 46.2° (200), and 67.5° (220) (JCPDS No. 040802).[28] Similar diffraction peaks were also observed on Pt/CNT@C-700 and Pt/CNT@CN-700 (Figure S4). However, the intensities of diffraction peaks for the metallic Pt of the two coated catalysts were much weaker than that of Pt/CNT due to the coating formed on the Pt/CNT surface.

To further examine the morphology of the coatings, TEM images of the catalysts are compared in Figure 1. For Pt/CNT,

https://doi.org/10.1021/acsami.1c05101
ACS Appl. Mater. Interfaces 2021, 13, 29541−29550

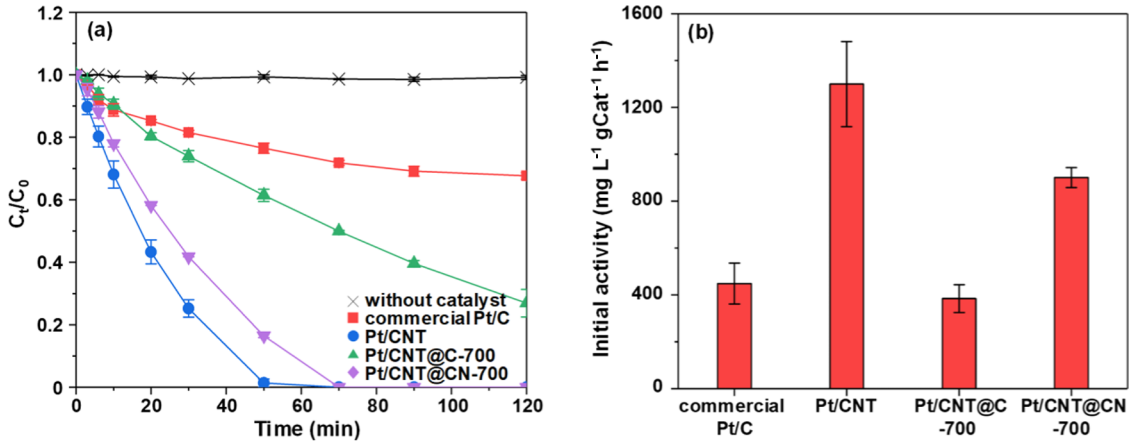

Figure 2. Superior catalytic hydrogenation reduction of Se(IV) by Pt/CNT@CN. (a) Reduction kinetics. (b) Initial activities. C_0 and C_t are the Se(IV) concentrations at reaction times zero and t, respectively. Reaction conditions: 20 mg L^{-1} Se(IV), 200 mL min^{-1} H_2 flow, and 0.150 g L^{-1} catalyst in 10 mmol L^{-1} HAc-NaAc buffer (pH 4.75). Error bars represent ± one standard deviation from the mean of triplicate samples.

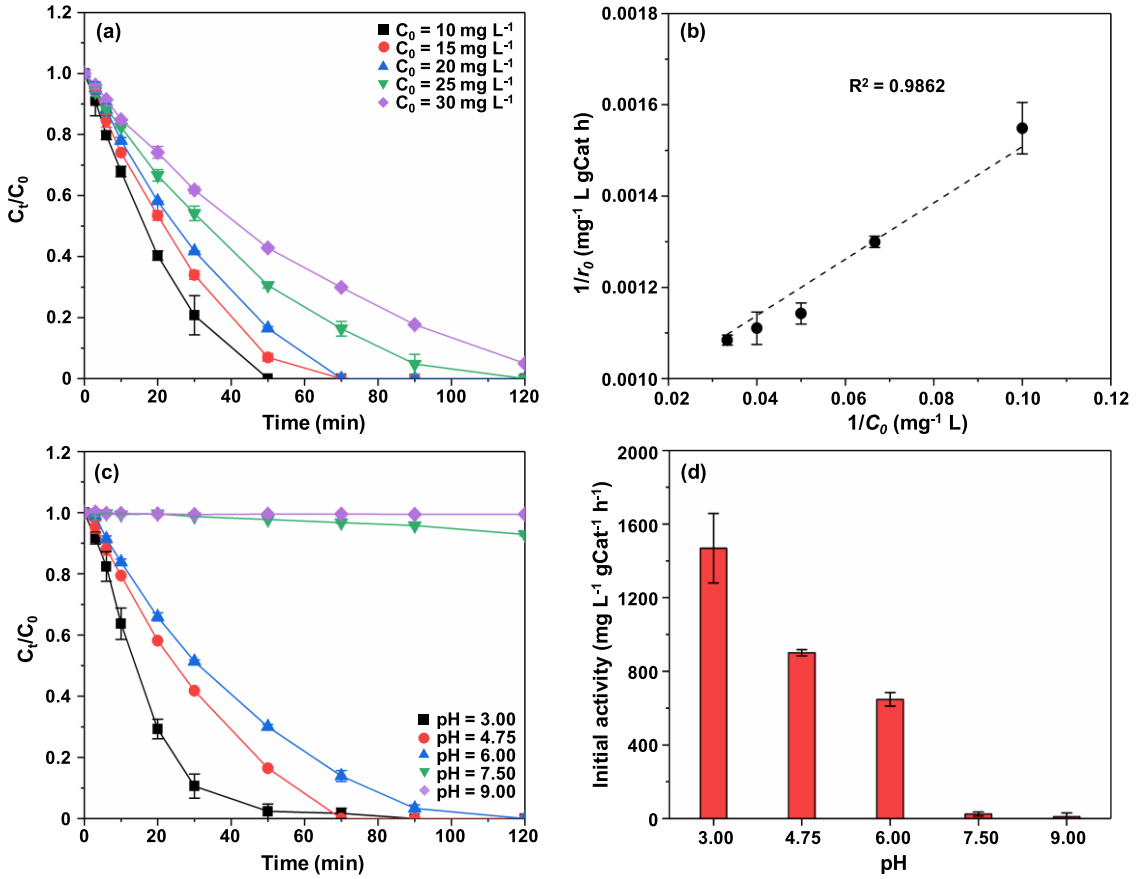

Figure 3. Effect of (a), (b) initial concentration (C_0) of Se(IV) and (c), (d) solution pH on the catalytic hydrogenation reduction of Se(IV) over Pt/CNT@CN-700. C_t is the Se(IV) concentration at reaction time t, and r_0 is the initial activity of the catalyst. Reaction conditions: 200 mL min^{-1} H_2 flow and 0.150 g L^{-1} catalyst in 10 mmol L^{-1} HAc-NaAc buffer (pH 4.75). Error bars represent standard deviations of triplicate experiments.

the CNT with a diameter of about 32 nm was distributed in the field of the vision and Pt particles were evenly riveted on the external surface of the CNT. For coated catalysts, homogeneous coating layers were visible on the surface of Pt/CNT. The average Pt particle sizes of the catalysts were calculated on the basis of the surface area-weighted diameter (see the calculation details in the SI), and the results are summarized in Table 1. The Pt particle sizes were 2.96, 4.52, and 4.71 nm for Pt/CNT, Pt/CNT@C-700, and Pt/CNT@CN-700, respectively.

Effective Catalytic Hydrogenation Reduction of Se(IV) to Se(0) on Pt/CNT@CN. The control experiment showed that Se(IV) concentration remained constant in the absence of Pt-based catalysts (Figure 2). The addition of Pt-based catalysts led to a marked reduction of Se(IV), indicating that the removal of Se(IV) is a catalytic reaction in nature. Soluble Se species were not detected in solution after the

https://doi.org/10.1021/acsami.1c05101
ACS Appl. Mater. Interfaces 2021, 13, 29541−29550

reaction (LOD for Se(IV) by ICP-MS = 0.04 μg L^{-1}, Figure S5), indicating that the reduction product was deposited on the surface of Pt/CNT@CN-700. The spent Pt/CNT@CN-700 was characterized (Figure S6). In the EDS mapping image (Figure S6a), the Se element was detected on the surface of the used Pt/CNT@CN-700. The XRD pattern (see Figure S6b) of the used Pt/CNT@CN-700 displayed new diffraction peaks at 23.5, 29.7, and 43.6° indexed to the (100), (101), and (102) planes of crystal Se(0), respectively,[18] indicative of the deposition of the reduction product Se(0) on the catalyst surface. Additionally, a sharp peak at 54.9 eV in the 3d region of the XPS spectrum of the used Pt/CNT@CN-700 (Figure S6c) further verified the formation and deposition of Se(0).[18,50] After complete reduction of 200 mL of 20 mg L^{-1} Se(IV) by Pt/CNT@CN-700, the increase of the catalyst mass due to elemental Se(0) deposition was 32.6 ± 0.5 mg, representing 96 ± 2% of the initial spiked Se(IV). The results clearly showed that Se(IV) was completely reduced to elemental Se(0) under the reaction conditions.

The Se(IV) reduction efficiency on different Pt-based catalysts was compared (Figure 2). The catalytic activities for the catalysts followed a decreasing order of Pt/CNT (r_0 = 1299.7 mg L^{-1} g_{cat}^{-1} h^{-1}) > Pt/CNT@CN-700 (900.5 mg L^{-1} g_{cat}^{-1} h^{-1}) > Pt/C (448.6 mg L^{-1} g_{cat}^{-1} h^{-1}) > Pt/CNT@C-700 (384.6 mg L^{-1} g_{cat}^{-1} h^{-1}). The high activity of Pt/CNT predominantly resulted from the exposed Pt particles that had a large amount of active Pt sites available for direct H_2 activation and Se(IV) reduction. The two coated catalysts (*i.e.*, Pt/CNT@CN-700 and Pt/CNT@C-700) also catalyzed the reduction of Se(IV), although their Pt particles were completely embedded by the carbonaceous coatings (as reflected by their TEM images and negligible CO chemisorptions, Figure 1 and Table 1). For example, more than 80% of the initial Se(IV) was reduced within 50 min in the presence of Pt/CNT@CN-700. Within the time frame of the test (*i.e.*, 2 h), Se(IV) concentration was reduced from 20 mg L^{-1} to 38.5 ± 0.2 μg L^{-1} over Pt/CNT@CN-700, meeting the drinking water guidelines of Se suggested by the WHO and U.S. EPA.[7,8] When the reaction time was prolonged to 5 h (Figure S5), Se(IV) concentration was further reduced to 2.9 ± 0.1 μg L^{-1}, lower than the Se guideline for aquatic life.[9] Notably, despite the lack of exposed Pt sites, the activity of Pt/CNT@CN-700 was significantly higher than the commercial Pt/C. The catalytic activities of coated catalysts mainly stemmed from the Schottky−Mott effect, by which H_2 could be activated on the carbonaceous coating due to the formation of metal−carbon heterojunction in the catalysts.[51] Compared with the catalyst coated by pure carbon (*i.e.*, Pt/CNT@C-700), the r_0 of Pt/CNT@CN-700 was more than two times higher. This can be explained by the significantly higher adsorption affinity of Pt/CNT@CN-700 to Se(IV) (see the detailed discussion below).

Surface Adsorption Played an Important Role in Se(IV) Reduction on Pt/CNT@CN. To clarify the impact of Se(IV) adsorption on its reduction, catalytic hydrogenation of Se(IV) with varied initial concentrations (C_0) was carried out on Pt/CNT@CN-700 (Figure 3a,b). The r_0 value increased from 646.6 mg L^{-1} g_{cat}^{-1} h^{-1} to 922.2 mg L^{-1} g_{cat}^{-1} h^{-1} as C_0 increased from 10 to 30 mg L^{-1}, consistent with the expectation that the reduction rate of Se(IV) was positively related to its concentration adsorbed on the Pt/CNT@CN-700 surface. The reaction data were further fitted to the Langmuir−Hinshelwood kinetics model. This model assumes that the reaction process is controlled by the reaction of sorbed reactants on the catalyst surface, wherein the reaction rate is proportional to the surface coverage of reactants[52,53]

$$r_0 = k\theta_s = k\frac{bC_0}{1 + bC_0} \quad (1)$$

$$\frac{1}{r_0} = \frac{1}{kbC_0} + \frac{1}{k} \quad (2)$$

where k is the reaction rate constant and θ_s is the coverage of the reactant on the catalyst surface. The reduction of Se(IV) on Pt/CNT@CN-700 can be well described by the Langmuir−Hinshelwood model, as suggested by the high linear correlation (R^2 = 0.99, Figure 3b) between $1/r_0$ and $1/C_0$. Thus, conversion of adsorbed Se(IV) on the catalyst surface was the rate-controlling step.[28] The results suggest that the effective Se(IV) adsorption on the catalyst surface favored its catalytic conversion.

The pivotal role of surface adsorption in the catalytic reduction of Se(IV) on Pt/CNT@CN-700 was further probed by the pH-effect experiments (Figure 3c,d). Increasing the reaction pH from 3.0 to 9.0 resulted in a monotonically decreased r_0 from 1468.5 to 10.6 mg L^{-1} g_{cat}^{-1} h^{-1} for Se(IV) reduction on Pt/CNT@CN-700. Such a strong pH dependency of the catalytic activity could be interpreted in terms of electrostatic interactions between the Pt/CNT@CN-700 surface and anionic Se(IV). Pt/CNT@CN-700 had a PZC of 7.24 (Figure S7 and Table 1). At the low reaction pH (*e.g.*, pH 3.0), the surface of Pt/CNT@CN-700 was positively charged due to the protonation effect, which enhanced the adsorption of anionic Se(IV) by electrostatic attraction. As a result, enhanced catalytic activity was observed. In contrast, the Pt/CNT@CN-700 surface was negatively charged at high pH (*e.g.*, pH 9.0), thus suppressing the adsorption of anionic Se(IV) due to electrostatic repulsion. Accordingly, catalytic Se(IV) reduction was markedly suppressed at high pH.

The dependency of Se(IV) reduction on the surface adsorption process also explains the significantly higher catalytic activity of Pt/CNT@CN-700 than Pt/CNT@C (Figure 2). Due to the presence of N-containing functional groups (*e.g.*, pyridinic N and pyrrolic N, Figure S3 and Table S3), Pt/CNT@CN-700 had a higher PZC (7.24) than that of Pt/CNT@C (3.05, Table 1). It was positively charged at the examined experimental pH (*e.g.*, 4.75), and thus resulted in electrostatic attraction to anionic Se(IV). In contrast, Pt/CNT@C-700 was negatively charged, which repelled Se(IV). Moreover, the presence of N-containing groups increased the surface hydrophilicity of Pt/CNT@CN-700, thus further facilitating the adsorption of hydrophilic Se(IV). The higher hydrophilicity of Pt/CNT@CN-700 was confirmed by its small water contact angle (59.1°) than that of Pt/CNT@C-700 (125.3°, Table 1 and Figure S8). As a result, favorable Se(IV) adsorption and hence much higher catalytic activity was achieved on Pt/CNT@CN-700 than Pt/CNT@C-700. Consistently, under the same adsorption conditions (10 μg L^{-1} Se(IV) and 0.150 g L^{-1} catalyst at pH 4.75 and 25.0 °C for 24 h), the adsorption coefficient (K_d) of Se(IV) on Pt/CNT@CN-700 (6.2 L g^{-1}) was significantly higher than that of Pt/CNT@C-700 (0.1 L g^{-1}, Figure S9a).

Coating Properties Significantly Affect Se(IV) Reduction on Pt/CNT@CN. To probe the effect of coating properties on the activity of Pt/CNT@CN, we studied the catalytic reduction of Se(IV) on Pt/CNT@CN prepared under

https://doi.org/10.1021/acsami.1c05101
ACS Appl. Mater. Interfaces 2021, 13, 29541−29550

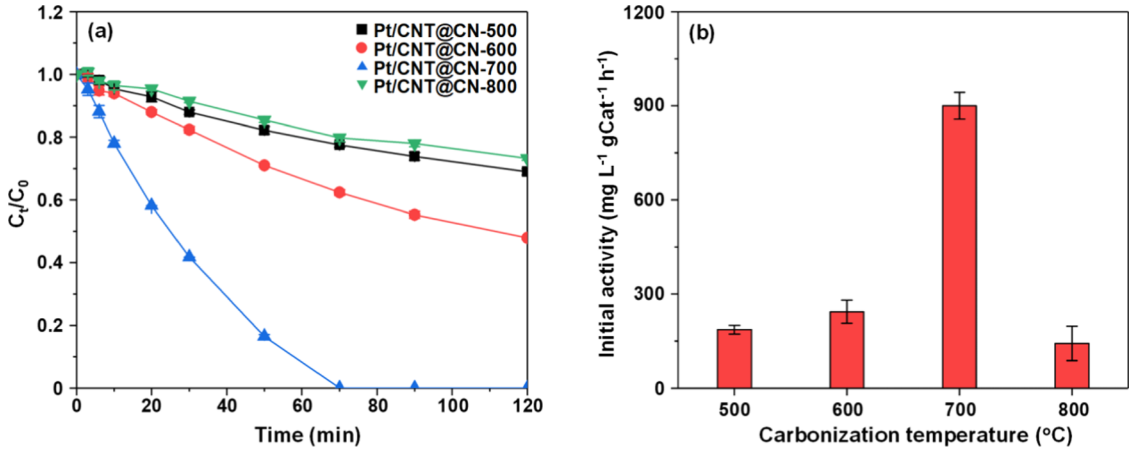

Figure 4. Carbonization temperature affected the catalytic hydrogenation reduction of Se(IV) on Pt/CNT@CN. (a) Reduction kinetics. (b) Initial activities. C_0 and C_t are the Se(IV) concentrations at reaction times zero and t, respectively. Reaction conditions: 20 mg L^{-1} Se(IV), 200 mL min^{-1} H_2 flow and 0.150 g L^{-1} Pt/CNT@CN in 10 mmol L^{-1} HAc-NaAc buffer (pH 4.75). Error bars represent ± one standard deviation from the mean of triplicate samples.

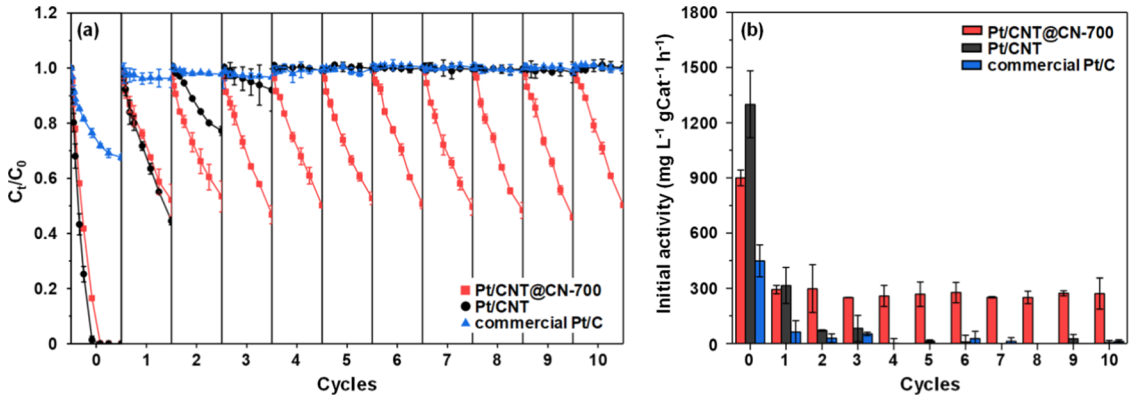

Figure 5. Stable catalytic hydrogenation reduction of Se(IV) on Pt/CNT@CN. (a) Consecutive reduction kinetics. (b) Initial activities. C_0 and C_t are the Se(IV) concentrations at reaction times zero and t, respectively. Reaction conditions: 20 mg L^{-1} Se(IV), 200 mL min^{-1} H_2 flow, and 0.150 g L^{-1} catalyst in 10 mmol L^{-1} HAc-NaAc buffer (pH 4.75). Error bars represent ± one standard deviation from the mean of triplicate samples.

different carbonization temperatures. The catalytic activities of Pt/CNT@CN varied significantly with the carbonization temperature (Figure 4). More than 95% of Se(IV) can be removed on Pt/CNT@CN-700 within 70 min. The Se(IV) removal was 31, 52, and 27% on Pt/CNT@CN-500, Pt/CNT@CN-600, and Pt/CNT@CN-800, respectively, after reaction for 120 min. The r_0 values were 186.6, 244.0, 900.5, and 142.7 mg L^{-1} g_{cat}^{-1} h^{-1} for Pt/CNT@CN-500, Pt/CNT@CN-600, Pt/CNT@CN-700, and Pt/CNT@CN-800, respectively. There is a volcano-type dependence of catalytic activity on the carbonization temperature.

The catalytic activity of Pt/CNT@CN for Se(IV) reduction was mainly controlled by conductivity, the N content, and hydrophilicity of the catalyst coatings. Raman spectra analyses and the EIS test were conducted to characterize the graphitization degree and the charge-transfer resistance of the catalysts. Surface properties, including N-containing groups and hydrophilicity, were determined by XPS and by the measurement of the static contact angle. The results showed that I_D/I_G value and charge-transfer resistance (R_{ct}) sharply decreased with the increase of the carbonization temperature from 500 to 800 °C (Figures S10 and S11 and Table S3), indicating that the thermal treatment effectively enhances the graphitization degree and thus improves the electron conductivity of Pt/CNT@CN.[31,54,55] Furthermore, the thermal treatment led to the conversion of pyridinic N and pyrrolic N to graphitic N and surface hydrophilicity to hydrophobicity due to the loss of N- and O-containing functionalities (Figures S3 and S8 and Table S3), resulting in drastically decreased adsorption sites for Se(IV). The interplay between the enhanced electron conductivity and reduced surface hydrophilicity with increasing carbonization temperature leads to the volcano-type dependence of catalytic activity on the carbonization temperature.

N-Doped Carbon Coating Significantly Enhanced Catalytic Stability. The catalytic stability was evaluated on commercial Pt/C, Pt/CNT, and Pt/CNT@CN-700 using ten cycles of catalyst reuse (Figure 5). The used catalysts were regenerated by various methods to remove the deposited Se(0), including high-temperature calcination and treating with carbon disulfide, NaOH, or mixed acid solution of HCl and HNO_3. Efficient regeneration can only be achieved using a mixed acid solution, as confirmed by the absence of Se(0) peaks in the XRD and XPS spectra of the regenerated catalyst (Figure S6b,c). After ten reaction cycles, the r_0 of Pt/CNT substantially decreased from 1299.7 to 5.7 mg L^{-1} g_{cat}^{-1} h^{-1}, losing 99% of its initial activity (Figure 5). The marked catalyst deactivation resulted from the Pt particle loss due to the weak

https://doi.org/10.1021/acsami.1c05101
ACS Appl. Mater. Interfaces 2021, 13, 29541−29550

metal−support interaction. This was supported by the ICP-AES measurement. It suggested that 92% of Pt in Pt/CNT was lost during the hydrogenation reaction and regeneration treatment processes (Table 1). Significant deactivation was also observed for the commercial Pt/C catalyst, with approximately 85% of its initial activity lost after the first use.

In contrast to commercial Pt/C and Pt/CNT, Pt/CNT@CN-700 exhibited good stability. The fresh Pt/CNT@CN-700 had an r_0 value of 900.5 mg L^{-1} g_{cat}^{-1} h^{-1}. The r_0 of the catalyst decreased to 293.0 mg L^{-1} g_{cat}^{-1} h^{-1} after the first use but remained constant in the following reaction cycles, indicating the good stability of Pt/CNT@CN-700. The results of ICP-AES showed that the Pt content in the used Pt/CNT@CN-700 was almost identical to the fresh one (Table 1). Meanwhile, similar Pt particle distribution was identified on the used catalyst as that of the fresh one (Figure 1), confirming the effective protection of Pt particles by CN coating. The regeneration using mixed acid can result in the surface oxidation of the CN coating. As a result, O-containing functionalities were introduced, giving rise to a low PZC (decreased from 7.24 to 5.21 after use) and suppressed the electrostatic attraction interaction between Se(IV) and the catalyst surface. Hence, a lower catalyst activity of the used Pt/CNT@CN-700 was observed. After the first reaction cycle, the catalytic activity of Pt/CNT@CN-700 was stable and no further catalyst deactivation was observed, indicating that further surface oxidation was not significant in the consecutive reaction cycles. Note that the catalytic activity of Pt/CNT@CN-700 was more than four times higher than those of Pt/C and Pt/CNT after two cycles, and was more than 20 times higher after ten cycles (Figure 5). This highlights the promising advantages of Pt/CNT@CN due to the effective protection of Pt particles from CN coating.

Catalytic Reduction of Se(IV) on Pt/CNT@CN in Spiked Water Samples. To verify the practical applicability, the catalytic Se(IV) reduction over Pt/CNT@CN-700 was conducted in three different spiked water samples. Se(IV) was effectively reduced on Pt/CNT@CN-700 in all spiked samples (Figure S12a). After reaction for 70 min, Se(IV) was removed by 79, 37, and 39% in tap water, well water, and Xuanwu Lake water, respectively. The Se(IV) reduction efficiencies in the two spiked natural water samples (*i.e.*, well water and lake water) were significantly lower than that in deionized water (removed by 95% within 70 min). As mentioned above, the Se(IV) reduction rate was strongly dependent on its adsorption to Pt/CNT@CN-700. Compared with deionized water, the two natural water samples had higher salinity (in the range of 0.15−0.27 PSU) and dissolved organic matter (DOM) content (TOC in the range of 2.71−6.24 mg L^{-1}, Table S1). The presence of coexisting anions and DOM may compete with Se(IV) for the adsorption sites,[56,57] resulting in decreased Se(IV) adsorption on Pt/CNT@CN-700. As shown in Figure S9b, given the same Se(IV) initial concentration (10 μg L^{-1}), the adsorption ratio of Se(IV) to Pt/CNT@CN-700 gradually decreased when the concentration of coexisting anions increased. The adsorption ratio decreased from 48 to 36, 29, 28, and 41% in the presence of 10 mg L^{-1} Cl^-, CO_3^{2-}, SO_4^{2-}, and PO_4^{3-}, respectively. SO_4^{2-} was particularly competitive, likely due to its similar structure with the Se(IV) anion and more negative charge that facilitated the electrostatic attraction adsorption.[58−60] The catalytic activity of Pt/CNT@CN-700 in the tap water sample, which had lower contents of anions and DOM, was remarkably higher than that in the two natural water samples. The r_0 of Pt/CNT@CN-700 in tap water was determined to be 825.1 mg L^{-1} g_{cat}^{-1} h^{-1}, comparable with that in deionized water (900.5 mg L^{-1} g_{cat}^{-1} h^{-1}). In spiked tap water, the catalytic activity of Pt/CNT@CN-700 was five times higher than that of commercial Pt/C (r_0 = 153.7 mg L^{-1} g_{cat}^{-1} h^{-1}).

CONCLUSIONS

Se(IV) is a common toxic pollutant from both natural and anthropogenic sources, and reductive treatment is a sound approach to diminish its risks in water. Here, we demonstrate a promising novel approach to remove Se(IV) *via* the H_2-based catalytic reduction, using a stable Pt/CNT catalyst coated by N-doped carbon. Such coated catalysts have unique surface-active sites due to the formation of Schottky−Mott type Pt-carbon heterojunction. N-doping of the coating enhances proximal Se(IV) adsorption and concentration near catalytic sites, which likely helps overcome inefficiencies associated with the catalytic treatment of low concentration of target pollutants commonly encountered in the drinking water treatment.[61,62] Moreover, the catalyst overcomes conventional catalyst deactivation from the blocking effect from the deposition of insoluble Se(0) product and Pt loss during reaction and catalyst regeneration. Reduction of some other pollutants (*e.g.*, Hg^{2+} and Ni^{2+}, *etc.*) also forms insoluble products depositing on the catalyst surface, commonly leading to catalyst deactivation.[63−65] Additionally, catalyst deactivation due to the loss of active noble metals during the reaction and regeneration processes[51,66,67] is a common and significant hindrance to the application of catalysis in water treatment. Thus, coating technology in catalyst preparation may open up opportunities for the catalysis avenues applied in some pollutant reduction processes, in which conventional supported noble catalysts are currently unfeasible. Our results also suggest that natural water constituents, such as ions and DOM, can compete with target pollutants for adsorption sites on coated catalysts and thus reduce their catalytic activity. Catalytic reduction using coated catalysts in natural waters may be improved by combining with normal drinking water treatment processes (*e.g.*, activated carbon adsorption) that can remove DOM constituents. Further investigation is needed to design coating materials with high adsorption selectivity for the target pollutants.

ASSOCIATED CONTENT

Supporting Information

The Supporting Information is available free of charge at https://pubs.acs.org/doi/10.1021/acsami.1c05101.

Preparation methods of Pt/CNT and Pt/CNT@C-700; detailed characterization method of Pt-based catalysts; concentration−time profiles of Se(IV) in solution in the absence of H_2 (Figure S1); results of catalyst dosage experiments (Figure S2 and Table S2); N 1s XPS spectra, XRD patterns, PZC titration curves, static water contact angle measurements, Raman spectra, and Nyquist diagrams obtained in the EIS test for different Pt-based catalysts (Figures S3, S4, S7, S8, S10, and S11); long-time catalytic hydrogenation reduction of Se(IV) over Pt/CNT@CN-700 (Figure S5); characterization results of Pt/CNT@CN-700 after use and after regeneration (Figure S6); adsorption ratios of Se(IV) to coated catalysts with and without the co-existing

https://doi.org/10.1021/acsami.1c05101
ACS Appl. Mater. Interfaces 2021, 13, 29541−29550

anions (Figure S9); catalytic hydrogenation reduction of Se(IV) on Pt/CNT@CN-700 in spiked water samples (Figure S12); sample characteristics of water samples (Table S1); summary of the coating properties of Pt/CNT@CN catalysts (Table S3); and determination method of average Pt particle sizes (PDF)

AUTHOR INFORMATION

Corresponding Author

Heyun Fu − *State Key Laboratory of Pollution Control and Resource Reuse/School of the Environment, Nanjing University, Nanjing, Jiangsu 210046, China;* orcid.org/0000-0002-0014-1829; Phone: +86-025-8968-0373; Email: heyunfu@nju.edu.cn

Authors

Yuhan Sun − *State Key Laboratory of Pollution Control and Resource Reuse/School of the Environment, Nanjing University, Nanjing, Jiangsu 210046, China*

Minghui Li − *State Key Laboratory of Pollution Control and Resource Reuse/School of the Environment, Nanjing University, Nanjing, Jiangsu 210046, China*

Xiaolei Qu − *State Key Laboratory of Pollution Control and Resource Reuse/School of the Environment, Nanjing University, Nanjing, Jiangsu 210046, China;* orcid.org/0000-0002-9157-4274

Shourong Zheng − *State Key Laboratory of Pollution Control and Resource Reuse/School of the Environment, Nanjing University, Nanjing, Jiangsu 210046, China;* orcid.org/0000-0001-8660-4910

Pedro J. J. Alvarez − *Department of Civil and Environmental Engineering, Rice University, Houston, Texas 77005, United States;* orcid.org/0000-0002-6725-7199

Complete contact information is available at: https://pubs.acs.org/10.1021/acsami.1c05101

Notes

The authors declare no competing financial interest.

ACKNOWLEDGMENTS

This work was supported by the Natural Science Foundation of Jiangsu Province (Grant BK20190059), the National Key Research and Development Program of China (Grant 2019YFC1804201), and the National Natural Science Foundation of China (Grant 21976086). P.J.J.A. was partially supported by the US National Science Foundation (NSF) Engineering Research Center for Nanotechnology-Enabled Water Treatment (Grant EEC-1449500).

REFERENCES

(1) Foster, L. H.; Sumar, S. Selenium in the environment, food and health. *Nutr. Food Sci.* **1995**, *95*, 17−23.

(2) Burau, R. G. Environmental chemistry of selenium. *Calif. Agric.* **1985**, *39*, 16−18.

(3) Andrahennadi, R.; Wayland, M.; Pickering, I. J. Speciation of selenium in stream insects using X-ray absorption spectroscopy. *Environ. Sci. Technol.* **2007**, *41*, 7683−7687.

(4) Sharma, S.; Singh, R.; Nielson, G. G. Selenium in soil, plant, and animal systems. *CRC Crit. Rev. Environ. Control* **1983**, *13*, 23−50.

(5) Fordyce, F. M. *Selenium Deficiency and Toxicity in the Environment*; Selinus, O.; Alloway, B.; Centeno, J. A.; Finkelman, R. B.; Fuge, R.; Lindh, U.; Smedley, P., Eds.; Springer: Dordrecht, 2013; pp 375−416.

(6) Feng, L.; Chen, W.; Li, J.; Day, G.; Drake, H.; Joseph, E.; Zhou, H. Biological antagonism inspired detoxification: removal of toxic elements by porous polymer networks. *ACS Appl. Mater. Interfaces* **2019**, *11*, 14383−14390.

(7) World Health Organization. *Guidelines for Drinking-Water Quality*; WHO Press: Geneva, Switzerland, 2011.

(8) United States Environmental Protection Agency. *Basic Information about Selenium in Drinking Water*. http://water.epa.gov/drink/contaminants/basicinformation/selenium.cfm (accessed 2014).

(9) United States Environmental Protection Agency. *Aquatic Life Ambient Water Quality Criterion for Selenium − Freshwater*; EPA-822-R-16-006, 2016.

(10) Khan, K. U.; Zuberi, A.; Fernandes, J.; Ullah, I.; Sarwar, H. An overview of the ongoing insights in selenium research and its role in fish nutrition and fish health. *Fish Physiol. Biochem.* **2017**, *43*, 1689−1705.

(11) Wayland, M.; Casey, R.; Woodsworth, E. A dietary assessment of selenium risk to aquatic birds on a coal mine affected stream in Alberta, Canada. *Hum. Ecol. Risk Assess. Int. J.* **2007**, *13*, 823−842.

(12) Mehdi, Y.; Hornick, J.; Istasse, L.; Dufrasne, I. Selenium in the environment, metabolism and involvement in body functions. *Molecules.* **2013**, *18*, 3292−3311.

(13) Mangiapane, E.; Pessione, A.; Pessione, E. Selenium and selenoproteins: an overview on different biological systems. *Curr. Protein Pept. Sci.* **2014**, *15*, 598−607.

(14) Myneni, S. C. B.; Tokunaga, T. K.; Brown, G. E. Abiotic selenium redox transformations in the presence of Fe(II, III) oxides. *Science.* **1997**, *278*, 1106−1109.

(15) Devi, P.; Thakur, A.; Chopra, S.; Kaur, N.; Kumar, P.; Singh, N.; Kumar, M.; Shivaprasad, S. M.; Nayak, M. K. Ultrasensitive and selective sensing of selenium using nitrogen-rich ligand interfaced carbon quantum dots. *ACS Appl. Mater. Interfaces* **2017**, *9*, 13448−13456.

(16) Liang, L.; Yang, W.; Guan, X.; Li, J.; Xu, Z.; Wu, J.; Huang, Y.; Zhang, X. Kinetics and mechanisms of pH-dependent selenite removal by zero valent iron. *Water Res.* **2013**, *47*, 5846−5855.

(17) Zhang, J.; Wang, Y.; Shao, Z.; Li, J.; Zan, S.; Zhou, S.; Yang, R. Two selenium tolerant Lysinibacillus sp. strains are capable of reducing selenite to elemental Se efficiently under aerobic conditions. *J. Environ. Sci.* **2019**, *77*, 238−249.

(18) Bai, Y.; Wang, X.; Lu, Y.; Fu, L.; Zhang, F.; Lau, T.; Zeng, R. J. Microbial selenite reduction coupled to anaerobic oxidation of methane. *Sci. Total Environ.* **2019**, *669*, 168−174.

(19) Nguyen, V. N. H.; Amal, R.; Beydoun, D. Photocatalytic reduction of selenium ions using different TiO_2 photocatalysts. *Chem. Eng. Sci.* **2005**, *60*, 5759−5769.

(20) Tan, T.; Beydoun, D.; Amal, R. Effects of organic hole scavengers on the photocatalytic reduction of selenium anions. *J. Photochem. Photobiol., A* **2003**, *159*, 273−280.

(21) Ling, L.; Pan, B.; Zhang, W. Removal of selenium from water with nanoscale zero-valent iron: mechanisms of intraparticle reduction of Se(IV). *Water Res.* **2015**, *71*, 274−281.

(22) Xu, L.; Huang, Y. Kinetics and mechanism of selenite reduction by zero valent iron under anaerobic condition activated and enhanced by dissolved Fe(II). *Sci. Total Environ.* **2019**, *664*, 698−706.

(23) Li, Y.; Guo, X.; Dong, H.; Luo, X.; Guan, X.; Zhang, X.; Xia, X. Selenite removal from groundwater by zero-valent iron (ZVI) in combination with oxidants. *Chem. Eng. J.* **2018**, *345*, 432−440.

(24) Zhang, N.; Lin, L.; Gang, D. Adsorptive selenite removal from water using iron-coated GAC adsorbents. *Water Res.* **2008**, *42*, 3809−3816.

(25) Han, D. S.; Batchelor, B.; Abdel-Wahab, A. Sorption of selenium(IV) and selenium(VI) to mackinawite (FeS): effect of contact time, extent of removal, sorption envelopes. *J. Hazard. Mater.* **2011**, *186*, 451−457.

(26) Tan, L. C.; Nancharaiah, Y. V.; van Hullebusch, E. D.; Lens, P. N. L. Selenium: environmental significance, pollution, and biological treatment technologies. *Biotechnol. Adv.* **2016**, *34*, 886−907.

(27) Chen, X.; Huo, X.; Liu, J.; Wang, Y.; Werth, C. J.; Strathmann, T. J. Exploring beyond palladium: catalytic reduction of aqueous oxyanion pollutants with alternative platinum group metals and new mechanistic implications. *Chem. Eng. J.* **2017**, *313*, 745−752.
(28) Liu, H.; Yu, Q.; Fu, H.; Wan, Y.; Qu, X.; Xu, Z.; Yin, D.; Zheng, S. Pt supported on ordered microporous carbon as highly active catalyst for catalytic hydrodeiodination of iodinated X-ray contrast media. *Appl. Catal., B* **2018**, *222*, 167−175.
(29) Sun, J.; Zhang, J.; Fu, H.; Wan, H.; Wan, Y.; Qu, X.; Xu, Z.; Yin, D.; Zheng, S. Enhanced catalytic hydrogenation reduction of bromate on Pd catalyst supported on CeO_2 modified SBA-15 prepared by strong electrostatic adsorption. *Appl. Catal., B* **2018**, *229*, 32−40.
(30) Kartusch, C.; Krumeich, F.; Safonova, O.; Hartfelder, U.; Makosch, M.; Sá, J.; van Bokhoven, J. A. Redispersion of gold multiple-twinned particles during liquid-phase hydrogenation. *Acs Catal.* **2012**, *2*, 1394−1403.
(31) Li, M.; Sun, Y.; Tang, Y.; Sun, J.; Xu, Z.; Zheng, S. Efficient removal and recovery of copper by liquid phase catalytic hydrogenation using highly active and stable carbon-coated Pt catalyst supported on carbon nanotube. *J. Hazard. Mater.* **2020**, *388*, No. 121745.
(32) Zhao, J.; Matsune, H.; Takenaka, S.; Kishida, M. Reduction of selenate with hydrazine monohydrate over Pt catalysts in aqueous solution. *Chem. Eng. J.* **2017**, *308*, 963−973.
(33) Argyle, M. D.; Bartholomew, C. H. Heterogeneous catalyst deactivation and regeneration: a review. *Catalysts* **2015**, *5*, 145−269.
(34) Bartholomew, C. H. Mechanisms of catalyst deactivation. *Appl. Catal., A* **2001**, *212*, 17−60.
(35) Li, M.; He, J.; Tang, Y.; Sun, J.; Fu, H.; Wan, Y.; Qu, X.; Xu, Z.; Zheng, S. Liquid phase catalytic hydrogenation reduction of Cr(VI) using highly stable and active Pd/CNT catalysts coated by N-doped carbon. *Chemosphere* **2019**, *217*, 742−753.
(36) Hu, Y.; Gao, X.; Yu, L.; Wang, Y.; Ning, J.; Xu, S.; Lou, X. W. D. Carbon-coated CdS petalous nanostructures with enhanced photostability and photocatalytic activity. *Angew. Chem., Int. Ed.* **2013**, *52*, 5636−5639.
(37) Chen, B.; Li, F.; Huang, Z.; Yuan, G. Recyclable and selective nitroarene hydrogenation catalysts based on carbon-coated cobalt oxide nanoparticles. *Chemcatchem.* **2016**, *8*, 1132−1138.
(38) Kong, X.; Fang, Z.; Bao, X.; Wang, Z.; Mao, S.; Wang, Y. Efficient hydrogenation of stearic acid over carbon coated Ni Fe catalyst. *J. Catal.* **2018**, *367*, 139−149.
(39) Kong, L.; Lu, X.; Bian, X.; Zhang, W.; Wang, C. Constructing carbon-coated Fe_3O_4 microspheres as antiacid and magnetic support for palladium nanoparticles for catalytic applications. *ACS Appl. Mater. Interfaces* **2011**, *3*, 35−42.
(40) Jeon, I. Y.; Noh, H. J.; Baek, J. B. Nitrogen-doped carbon nanomaterials: synthesis, characteristics and applications. *Chem. Asian J.* **2020**, *15*, 2282−2293.
(41) Wu, C.; Chen, X.; Tang, L.; Wei, Q.; Wei, X.; Liang, J.; Wang, L. Rationally constructing A nano MOF-derived Ni and CQD embedded N-doped carbon nanosphere for the hydrogenation of petroleum resin at low temperature. *ACS Appl. Mater. Interfaces* **2021**, *13*, 10855−10869.
(42) Shen, Z.; Han, Y.; Liu, Y.; Qin, Y.; Xing, P.; Zhao, H.; Jiang, B. Understanding surface basic sites of catalysts: kinetics and mechanism of dehydrochlorination of 1,2-dichloroethane over N-doped carbon catalysts. *Catalysts* **2020**, *10*, No. 707.
(43) He, L.; Weniger, F.; Neumann, H.; Beller, M. Synthesis, characterization, and application of metal nanoparticles supported on nitrogen-doped carbon: catalysis beyond electrochemistry. *Angew. Chem., Int. Ed.* **2016**, *55*, 12582−12594.
(44) Lv, R.; Cui, T.; Jun, M.; Zhang, Q.; Cao, A.; Su, D. S.; Zhang, Z.; Yoon, S.; Miyawaki, J.; Mochida, I.; Kang, F. Open-ended, N-doped carbon nanotube-graphene hybrid nanostructures as high-performance catalyst support. *Adv. Funct. Mater.* **2011**, *21*, 999−1006.
(45) Zhou, J.; Han, Y.; Wang, W.; Zheng, S.; Zhu, D.; Xu, Z.; Wan, H.; Yin, D. Reductive removal of chloroacetic acids by catalytic hydrodechlorination over Pd/ZrO_2 catalysts. *Appl. Catal., B* **2013**, *134*−*135*, 222−230.
(46) Li, M.; Zhou, X.; Sun, J.; Fu, H.; Qu, X.; Xu, Z.; Zheng, S. Highly effective bromate reduction by liquid phase catalytic hydrogenation over Pd catalysts supported on core-shell structured magnetites: impact of shell properties. *Sci. Total Environ.* **2019**, *663*, 673−685.
(47) Zhang, J.; He, D.; Su, H.; Chen, X.; Pan, M.; Mu, S. Porous polyaniline-derived FeNxC/C catalysts with high activity and stability towards oxygen reduction reaction using ferric chloride both as an oxidant and iron source. *J. Mater. Chem. A.* **2014**, *2*, 1242−1246.
(48) Yuan, G.; Keane, M. A. Liquid phase catalytic hydrodechlorination of 2,4-dichlorophenol over carbon supported palladium: an evaluation of transport limitations. *Chem. Eng. Sci.* **2003**, *58*, 257−267.
(49) Belin, T.; Epron, F. Characterization methods of carbon nanotubes: a review. *Mater. Sci. Eng. B* **2005**, *119*, 105−118.
(50) Gonzalez-Gil, G.; Lens, P. N. L.; Saikaly, P. E. Selenite reduction by anaerobic microbial aggregates: microbial community structure, and proteins associated to the produced selenium spheres. *Front. Microbiol.* **2016**, *7*, No. 571.
(51) Fu, T.; Wang, M.; Cai, W.; Cui, Y.; Gao, F.; Peng, L.; Chen, W.; Ding, W. Acid-resistant catalysis without use of noble metals: carbon nitride with underlying nickel. *Acs Catal.* **2014**, *4*, 2536−2543.
(52) De Pedro, Z. M.; Casas, J. A.; Gomez-Sainero, L. M.; Rodriguez, J. J. Hydrodechlorination of dichloromethane with a Pd/AC catalyst: Reaction pathway and kinetics. *Appl. Catal., B* **2010**, *98*, 79−85.
(53) Pintar, A.; Batista, J.; Levec, J.; Kajiuchi, T. Kinetics of the catalytic liquid-phase hydrogenation of aqueous nitrate solutions. *Appl. Catal., B* **1996**, *11*, 81−98.
(54) Zheng, X.; Zhang, S.; Xu, J.; Wei, K. Effect of thermal and oxidative treatments of activated carbon on its surface structure and suitability as a support for barium-promoted ruthenium in ammonia synthesis catalysts. *Carbon* **2002**, *40*, 2597−2603.
(55) Song, J.; Sun, B.; Liu, H.; Ma, Z.; Chen, Z.; Shao, G.; Wang, G. Enhancement of the rate capability of $LiFePO_4$ by a new highly graphitic carbon-coating method. *ACS Appl. Mater. Interfaces* **2016**, *8*, 15225−15231.
(56) Pincus, L. N.; Rudel, H. E.; Petrović, P. V.; Gupta, S.; Westerhoff, P.; Muhich, C. L.; Zimmerman, J. B. Exploring the mechanisms of selectivity for environmentally significant oxo-anion removal during water treatment: A review of common competing oxo-anions and tools for quantifying selective adsorption. *Environ. Sci. Technol.* **2020**, *54*, 9769−9790.
(57) Shimabuku, K. K.; Paige, J. M.; Luna-Aguero, M.; Summers, R. S. Simplified modeling of organic contaminant adsorption by activated carbon and biochar in the presence of dissolved organic matter and other competing adsorbates. *Environ. Sci. Technol.* **2017**, *51*, 10031−10040.
(58) Zhang, N.; Gang, D.; Lin, L. S. Adsorptive removal of parts per million level selenate using iron-coated GAC adsorbents. *J. Environ. Eng.* **2010**, *136*, 1089−1095.
(59) Jegadeesan, G. B.; Mondal, K.; Lalvani, S. B. Adsorption of Se (IV) and Se (VI) using copper-impregnated activated carbon and fly ash-extracted char carbon. *Water, Air, Soil Pollut.* **2015**, *226*, No. 234.
(60) Yamani, J. S.; Lounsbury, A. W.; Zimmerman, J. B. Adsorption of selenite and selenate by nanocrystalline aluminum oxide, neat and impregnated in chitosan beads. *Water Res.* **2014**, *50*, 373−381.
(61) Chaplin, B. P.; Roundy, E.; Guy, K. A.; Shapley, J. R.; Werth, C. J. Effects of natural water ions and humic acid on catalytic nitrate reduction kinetics using an alumina supported Pd−Cu catalyst. *Environ. Sci. Technol.* **2006**, *40*, 3075−3081.
(62) Jiang, W.; Xia, X.; Han, J.; Ding, Y.; Haider, M. R.; Wang, A. Graphene modified electro-fenton catalytic membrane for in situ degradation of antibiotic florfenicol. *Environ. Sci. Technol.* **2018**, *52*, 9972−9982.

https://doi.org/10.1021/acsami.1c05101
ACS Appl. Mater. Interfaces 2021, 13, 29541−29550

(63) Lambert, A.; Drogui, P.; Daghrir, R.; Zaviska, F.; Benzaazoua, M. Removal of copper in leachate from mining residues using electrochemical technology. *J. Environ. Manage.* **2014**, *133*, 78−85.
(64) Gkika, E.; Troupis, A.; Hiskia, A.; Papaconstantinou, E. Photocatalytic reduction and recovery of mercury by polyoxometalates. *Environ. Sci. Technol.* **2005**, *39*, 4242−4248.
(65) Boudjahem, A. G.; Serge, M.; Michel, M.; Mohammed, M. B. Study of support effects on the reduction of Ni^{2+} ions in aqueous hydrazine. *Langmuir* **2004**, *20*, 208−213.
(66) Arends, I. W. C. E.; Sheldon, R. A. Activities and stabilities of heterogeneous catalysts in selective liquid phase oxidations: recent developments. *Appl. Catal., A* **2001**, *212*, 175−187.
(67) Yuan, G.; Keane, M. A. Liquid phase hydrodechlorination of chlorophenols over Pd/C and Pd/Al_2O_3: a consideration of HCl/catalyst interactions and solution pH effects. *Appl. Catal., B* **2004**, *52*, 301−314.

https://doi.org/10.1021/acsami.1c05101
ACS Appl. Mater. Interfaces 2021, 13, 29541−29550